

Two-dimensional field-effect transistors based on lateral heterojunctions of transition metal dichalcogenides: dissipative quantum transport modeling

Giuseppe Lovarelli, Fabrizio Mazziotti, Demetrio Logoteta and Giuseppe Iannaccone, *Fellow, IEEE*

Abstract—Reducing the contact resistance of field-effect transistors based on two-dimensional materials is one of the key improvements required to enable the integration of such transistors in an advanced semiconductor manufacturing process. Suitably designed lateral heterojunctions provide an opportunity to independently tailor the contact and channel properties in order to optimize contact resistance. Inspired by the recent experimental demonstration of a two-dimensional p -type Schottky barrier, here we use quantum transport simulations to estimate the performance of p -type transistors in which the channel consists of a lateral heterostructure of $\text{NbS}_2/\text{MoS}_2/\text{NbS}_2$ (semimetal-semiconductor-semimetal). We find that the gate alignment with the channel is a critical design parameter, strongly influencing the capability of the gate to modulate the Schottky barrier at the $\text{MoS}_2/\text{NbS}_2$ interface. This effect is also found to significantly affect the scaling behavior of the device.

Index Terms—Two-dimensional materials, field-effect transistors, lateral heterojunctions, transition metaldichalcogenides.

I. INTRODUCTION

THE possibility to use two-dimensional (2D) materials in an industrial complementary metal-oxide semiconductor (CMOS) process depends several factors, but few are as critical as the capability to fabricate low-resistance metal contacts. Unfortunately, 2D semiconductors tend to form high Schottky

This work was partially supported by the European Union Horizon 2020 Framework Programme under the “Quantum Engineering for Machine Learning” (QUEFORMAL) project (Grant Agreement No. 829035), by the by the Italian MIUR through the PRIN project FIVE2D and by the Italian Ministry of University and Research through the ForeLab Departments of Excellence Grant.

Giuseppe Lovarelli was with Dipartimento di Fisica, Università di Pisa, Largo Bruno Pontecorvo 3, 56127 Pisa, Italy and with Dipartimento di Ingegneria dell’Informazione, Università di Pisa, Via Girolamo Caruso 16, 56122 Pisa, Italy (e-mail: giuseppe.lovarelli@phd.unipi.it).

Fabrizio Mazziotti is with Dipartimento di Ingegneria dell’Informazione, Università di Pisa, Via Girolamo Caruso 16, 56122 Pisa, Italy (e-mail: f.mazziotti1@phd.unipi.it).

Demetrio Logoteta is with Dipartimento di Ingegneria dell’Informazione, Elettronica e Telecomunicazioni, Università di Roma La Sapienza, via Eudossiana 18, 00184, Roma, Italy, (e-mail: demetrio.logoteta@uniroma1.it).

Giuseppe Iannaccone is with Dipartimento di Ingegneria dell’Informazione, Università di Pisa, Via Girolamo Caruso 16, 56122 Pisa, Italy (e-mail: giuseppe.iannaccone@unipi.it).

barriers with bulk metals, and the difficulty in achieving high doping levels in monolayers hinders the adoption of the conventional approach based on thinning these barriers enough to make them transparent to carrier tunnelling [1]–[3].

Contacting semiconducting monolayers by defining vertical or lateral heterojunctions with 2D metals or quasi-metals has attracted significant interest [4]–[11], especially in the perspective of developing all-2D circuits where all circuit components, including metallizations and insulating regions, are based on 2D materials.

In vertical heterojunctions, monolayers are weakly coupled by van der Waals interactions. This prevents the undesired occurrence of interfacial spurious states and Fermi level pinning [1], [12]–[14]; however, the small coupling also entails low carrier injection [13]. On the other hand, the edge contact between monolayers in lateral heterojunctions is characterized by a stronger coupling due to the covalent character of the atomic bonds. Provided that the quality of the interface is controlled and the height of the Schottky barrier is low enough, this translates to potentially efficient carrier injection [15], [16].

The capability to engineer both n - and p -type contacts is another essential requirement to implement a CMOS technology. Unfortunately, realizing p -type field-effect transistors (FETs) based on 2D materials has proven extremely challenging, due to the strong influence of the commonly used dielectric substrates, that tend to induce an n -type doping in the channel and of Fermi level pinning at the conduction band [17]. In this respect, recent experiments have demonstrated the fabrication of p -type Schottky diodes based on a lateral heterojunction of NbS_2 and MoS_2 in their 2H-form [18]. The reported, significant, current modulation indicates an effective reduction of the parasitic resistance associated to the MoS_2 contact when the NbS_2 buffer region is included.

In this paper we study the physics and the performance perspectives of a p -type FET based on a monolayer MoS_2 channel connected to monolayer NbS_2 access regions through lateral heterojunctions, using quantum transport simulations and critical materials parameters calibrated with experiments as discussed in Ref. [18]. Our results indicate that the phonon-assisted interband tunneling at the $\text{NbS}_2/\text{MoS}_2$ interface plays a major role in determining device behavior. It also translates

into a pronounced sensitivity of the device to some architectural details, such as the alignment between the gate electrode and the channel, that should be carefully addressed in order to optimize performance.

We find that the 2D heterojunction FET is not competitive in terms of performance with silicon FETs for front-end devices, as can be observed by considering the IRDS (International Roadmap for Devices and Systems) [19], but it has very interesting performance in terms of devices suitable for 3D integration (i.e., the vertical stacking of planar layers of transistors), given that it can be fabricated with back-end-of-the-line (BEOL) processing [20].

The paper is organized as follows. In Section II, we present our model and our simulation approach. In Section III, we discuss our results in terms of the device physics, performance and optimization opportunities. Our concluding remarks are drawn in Section IV.

II. MODEL

Following Ref. [18], we model the isolated monolayers by means of the two-bands first-nearest neighbor tight-binding Hamiltonian

$$H_{2D,j}(\mathbf{k}) = \begin{pmatrix} E_{V,j} & t_j f_{2D}(\mathbf{k}) \\ t_j^* f_{2D}^*(\mathbf{k}) & E_{C,j} \end{pmatrix}, \quad (1)$$

where $E_{C,j}$ and $E_{V,j}$ are the conduction band minimum and valence band maximum, respectively, t_j is the hopping parameter, with $j = (\text{MoS}_2, \text{NbS}_2)$. In addition,

$$f_{2D}(\mathbf{k}) = 1 + 2 \cos\left(\frac{a}{2}k_x\right) e^{i\frac{\sqrt{3}}{2}k_y} \quad (2)$$

is the Bloch function that describes the periodicity of the hexagonal lattice with lattice constant a . Due to the relatively lower NbS_2 in-plane stiffness with respect to MoS_2 [21], [22], the channel was assumed unstrained, while the source and drain extensions were assumed compressively strained in the transverse direction. Accordingly, the lattice constant of NbS_2 was assumed the same as that of MoS_2 .

In agreement with the experimental and theoretical analyses in [18], the $\text{MoS}_2/\text{NbS}_2$ Schottky barrier height, i.e., the difference between μ_{NbS_2} , the electrochemical potential of NbS_2 , and the top of the MoS_2 valence band is 0.17 eV. Furthermore, the degeneracy of the NbS_2 conduction band is $\mu_{\text{NbS}_2} - E_{C,\text{NbS}_2} = 0.34$ eV. For the NbS_2 , the values of E_C , E_V and t were chosen in order to reproduce the density of states near the Fermi level E_F , while for the MoS_2 , we chose these parameters in order to reproduce the valence band curvature at the K -point.

As pointed out in [18], the exact value of the lattice constant of Nb-doped MoS_2 has a negligible influence on the band alignment with NbS_2 . Therefore, as a simplifying approximation, we considered it equal to the lattice constant of NbS_2 . The interface between the monolayers is assumed defectless and, according to the above-mentioned approximation, unstrained (see Fig. 1). As a zeroth-order approximation, the value of the hopping parameter between Mo and S atoms at the interface was assumed the same as in the free-standing monolayer. In practice, it can both increase or decrease with respect to

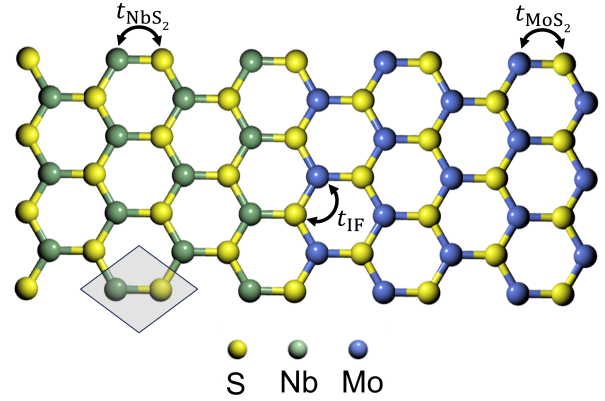


Fig. 1: Sketch of the $\text{MoS}_2/\text{NbS}_2$ heterointerface. The shaded region depicts the unit cell of the lattice. The tight-binding parameters are also indicated.

this value, but for small enough deviations the transmission through the interface will remain dominated by the Schottky barrier.

The hopping parameter t_{IF} between NbS_2 sulphur atoms and MoS_2 molybdenum atoms is assumed equal to t_{NbS_2} : due to the closeness between the values of t_{MoS_2} and t_{NbS_2} , no significant differences are expected by setting t_{IF} to t_{NbS_2} or to an intermediate value between t_{MoS_2} and t_{NbS_2} . We report the parameters of the model in Table I.

Transport simulations were performed within the non-equilibrium Green's function formalism [23] by using an in-house code [24], [25]. An orthorhombic elementary cell is designated to describe the system in real space in the direction of transport, and the device is assumed periodic in the lateral direction orthogonal to it. To sample the Brillouin zone along this transverse direction, a set of 100 transverse wave vectors were taken into account in simulations. In order to obtain a self-consistent solution, the transport equations were nonlinearly coupled with the 2D Poisson equation in the device cross section. The resulting system of equations was iteratively solved by adopting a fixed-point approach. Convergence was considered achieved when the maximum difference between the potential energy profile in consecutive iterations was less than 1 meV.

Electron-phonon scattering was included in the transport equations within the self-consistent Born approximation through diagonal self-energies [26] and by assuming an elastic and dispersionless approximation for acoustic and optical phonons, respectively. The optical phonon energy was obtained as the arithmetical average of the longitudinal, transverse and homopolar optical branches in MoS_2 , and set to $\hbar\bar{\omega} = 50$ meV [27]. Hole-phonon coupling was described within the deformation potential model. According to our long-wavelength approximation [28] and taking into account the suppression of the hole intervalley scattering in transition metal dichalcogenides due to the spin-valley locking effect [29], only the intravalley hole scattering at the K point was considered [30].

The values of the acoustic and optical deformation potentials (D_{op} and D_{ac} , respectively) are reported in Table I.

TABLE I: Tight-binding parameters and deformation potentials used in simulations

E_{V,NbS_2}	-5.59 eV
E_{C,NbS_2}	-0.34 eV
E_{V,MoS_2}	-0.17 eV
E_{C,MoS_2}	1.93 eV
t_{NbS_2}	-0.91 eV
t_{MoS_2}	-1.20 eV
$\hbar\omega_{\text{ph}}$	0.05 eV
D_{op}	4.6×10^8 eV/cm [30]
D_{ac}	2.5 eV [30]

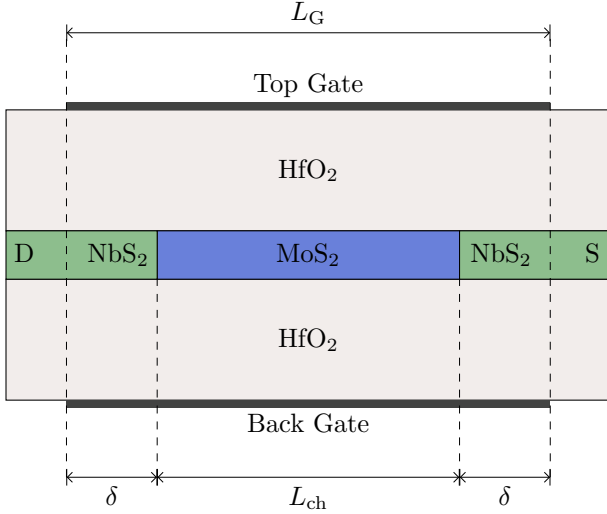


Fig. 2: Sketch of the cross section of the NbS₂/MoS₂/NbS₂ transistor.

III. RESULTS AND DISCUSSION

The cross-section of the NbS₂/MoS₂/NbS₂ transistor is sketched in Fig. 2. The current flow is controlled by means of a top and a bottom gate, separated from the channel by a 3.4 nm-thick HfO₂ layer with relative permittivity $\epsilon_r = 20$. The gate length L_G can be larger or smaller than the MoS₂ channel length L_{ch} ; this difference is quantified by the algebraic parameter $\delta = (L_G - L_{\text{ch}})/2$. The part of the NbS₂ source (S) and drain (D) extensions included in the domain of the Poisson equation are 12 nm long. Further enlarging these regions does not modify the simulation results. According to the estimates in Ref. [18], the MoS₂ channel is *p*-doped at a concentration $6 \times 10^{12} \text{ cm}^{-2}$.

Fig. 3a illustrates the transfer characteristics of the transistor for $L_{\text{ch}} = 20$ nm, $\delta = 0$ and different values of V_{DS} . A pronounced maximum of the current is observed, that shifts towards more negative V_{GS} as $|V_{\text{DS}}|$ increases. This effect can be explained with the help of Fig. 3b, that reports the band diagram of the transistor (central panel) for $V_{\text{DS}} = -0.15$ V and three values of V_{GS} , located before, at, and after the current peak. The corresponding local density of states (LDOS) in the middle of the channel is shown in the left panel of the figure, while the right panel presents a magnified view of the band diagram close to the MoS₂/NbS₂ interface at the source. The LDOS exhibits a peak, corresponding to

the local flattening of the MoS₂ valence band at the *M* point. The current is mainly limited by two factors: the density of available states in the channel between the source and drain electrochemical potentials (grey stripe in Fig. 3b), and the width of the tunneling barrier at the source-channel interface. As the gate voltage is swept through the current peak, the barrier thins, while the density of states decreases. The competition between the two phenomena induces the current peak.

When $|V_{\text{DS}}|$ increases, the tunneling barrier at the source/channel interface at a given energy widens. As a consequence, more negative gate voltages are needed to reach the current peak.

At $V_{\text{DS}} = -0.8$ V and -0.6 V, the $I_{\text{ON}}/I_{\text{OFF}}$ ratio equals 2330 and 1290, respectively. These values are obtained by setting $I_{\text{OFF}} = 0.1 \mu\text{A}/\mu\text{m}$ [19] and computing I_{ON} at $V_{\text{GS}} = V_{\text{GS,OFF}} + V_{\text{DS}}$, where $V_{\text{GS,OFF}}$ is the gate voltage at which $I_{\text{D}} = I_{\text{OFF}}$. We maintain these definitions through the paper.

The output characteristics of the transistor with $L_{\text{ch}} = 20$ nm are reported in Fig. 3c. An excellent current saturation at large bias is observed. Furthermore, we can observe that at low $|V_{\text{DS}}|$ the curve at $V_{\text{GS}} = -1.1$ V intersects with the curve at lower V_{GS} . This is simply due to the presence of the peak in the $I - V_{\text{GS}}$ characteristics shown in Figure 3b. Fig. 3d shows the band diagram along the device for several values of V_{GS} , which confirms an almost perfect electrostatic control of the gate over the channel potential, corresponding to a gate efficiency $\partial E_{\text{V}}/\partial V_{\text{GS}} \simeq 0.98$, where E_{V} is the top of the valence band at the center of the channel.

Despite this almost ideal electrostatic control of the gate over the channel, the subthreshold swing of the device is about 95 mV/dec and is thus degraded with respect to the thermionic limit of 60 mV/dec. This is a direct consequence of the carrier energy relaxation due to phonon emission, which allows interband electron transmission at the channel-drain interface also when the top of the valence band in the middle of the channel is pushed below the lower edge of the NbS₂ band. This effect is illustrated in Fig. 3e, which reports the current spectral density when the device operates in the subthreshold region.

In Fig. 4a we explore the scaling behavior of the transistor. The transfer characteristics are almost overlapping for $L_G > 10$ nm, while significant performance degradation is observed for $L_G = 5$ nm. In this case, the subthreshold swing increases to ~ 250 mV/dec and the $I_{\text{ON}}/I_{\text{OFF}}$ ratio correspondingly drops to 740 and 300 for $V_{\text{DS}} = -0.8$ V and $V_{\text{DS}} = -0.6$ V, respectively (see Table II). Also, the output resistance undergoes a large decrease, settling to $\sim 12 \text{ k}\Omega \cdot \mu\text{m}$ at $V_{\text{DS}} = V_{\text{GS}} = -0.6$ V (see Fig. 4b). The performance drop can be traced back to a strongly reduced capability of the gates to modulate the channel potential, as illustrated in panel Fig. 4c. Quantitatively, for $L_{\text{ch}} = 5$ nm the gate efficiency reduces to 0.57. Another marker of performance degradation as the channel length shrinks, is the threshold voltage roll-off ΔV_T with respect to the $L_{\text{ch}} = 20$ nm case, which is reported in Table III for the other considered values of L_{ch} .

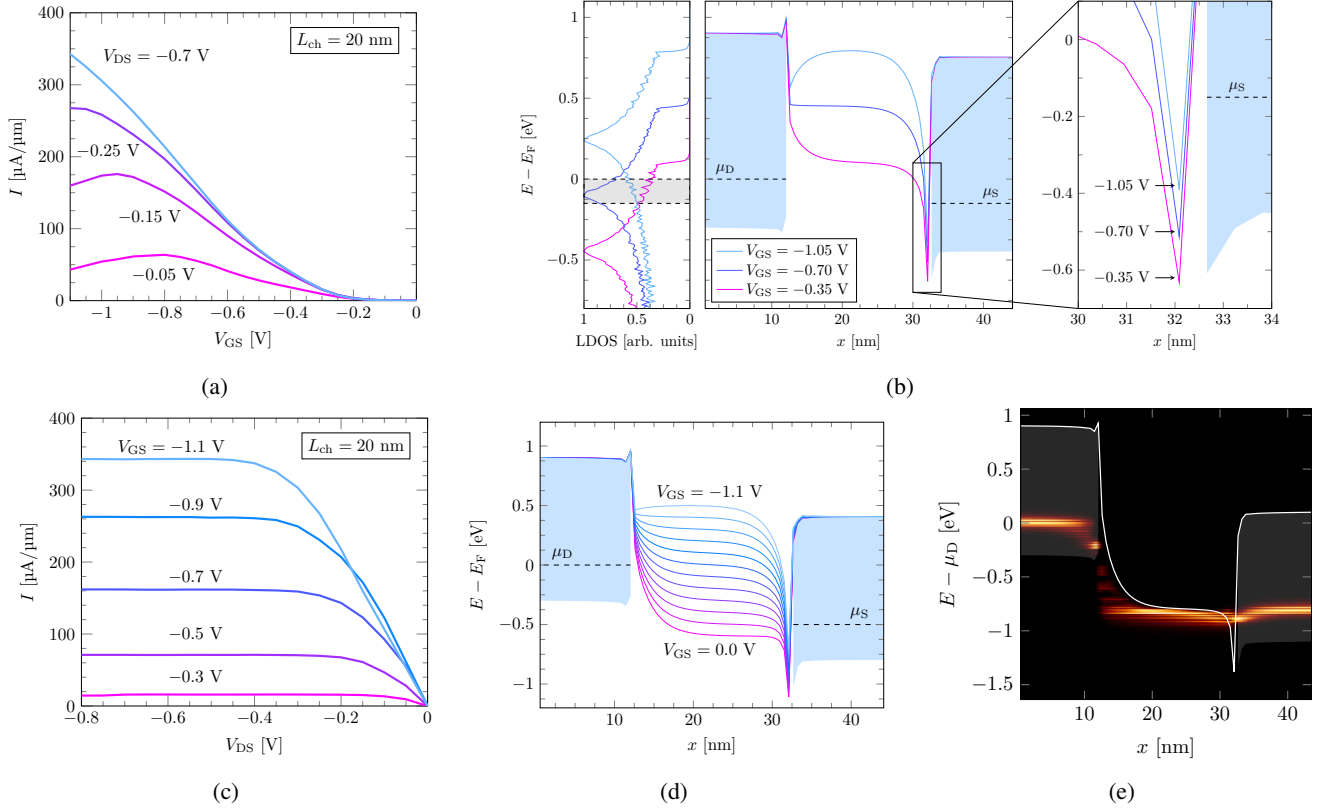


Fig. 3: (a) Transistor transfer characteristics for different values of V_{DS} . (b) Band diagram along the device (center panel) and local density of states in the center of the channel (left panel) at $V_{DS} = -0.15$ V and for three V_{GS} values close to the current peak. The blue-colored regions cover the energy window of the NbS_2 band involved in transport. The right panel is an enlargement of the band diagram close to the channel/source interface. (c) Transistor output characteristics. (d) Band diagram along the device for several values of V_{GS} . (e) Current spectrum at $V_{DS} = -0.8$ V and $V_{GS} = 0.1$ V. For all the panels, $L_{ch} = 20$ nm.

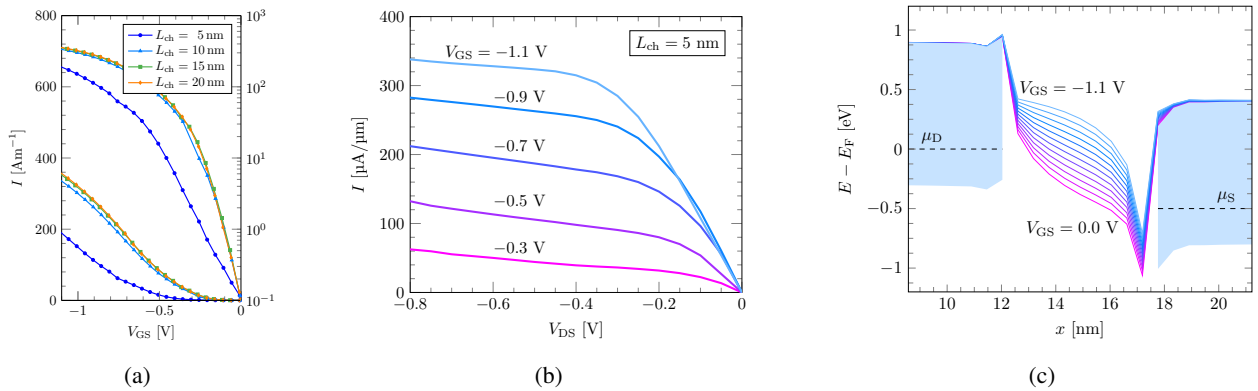


Fig. 4: (a) Transistor transfer characteristics for different channel lengths $L_{ch} = 5, 10, 15, 20$ nm. (b) Output characteristics for $L_{ch} = 5$ nm. (c) Band diagram at $L_{ch} = 5$ nm for several values of V_{GS} , at $V_{DS} = -0.5$ V.

TABLE II: I_{ON}/I_{OFF} at $V_{DS} = -0.6$ and -0.8 V ratio for different channel lengths.

V_{DS} [V]	L_{ch} [nm]	I_{ON}/I_{OFF}
-0.6	5	300
-0.6	10	1180
-0.6	15	1280
-0.6	20	1290
-0.8	5	740
-0.8	10	2130
-0.8	15	2300
-0.8	20	2330

TABLE III: Threshold voltage roll-off ΔV_T for different channel lengths.

L_{ch} [nm]	ΔV_T [V]	
	@ $V_{DS} = -0.6$ V	@ $V_{DS} = -0.8$ V
5	0.16	0.25
10	0.02	0.05
15	0.01	0.03

The effect of gate overlaps and underlaps on the I_{ON}/I_{OFF} ratio for $L_{ch} = 15$ nm is reported in Table IV. As one expects, the presence of overlaps has the effect of improving the I_{ON}/I_{OFF} ratio, as it results in a better electrostatic control over the channel potential; conversely, the presence of underlaps is detrimental to the device performance. More importantly, a comparison between Table II and Table IV highlights that the impact of the gate overlap (underlap) is much stronger than an equivalent gate extension (reduction) with $\delta = 0$. For instance, an increase of L_G from 10 nm to 15 nm by symmetrically including 2.5 nm-long overlaps on the source and drain sides, results in a 30% improvement of the I_{ON}/I_{OFF} ratio, while an equivalent extension of L_G with $\delta = 0$ only results in a 8% improvement. Analogously, a decrease of L_G from 15 nm to 10 nm by symmetrically including 2.5 nm-long underlaps on the source and drain sides degrades the I_{ON}/I_{OFF} ratio by 48%, while an equivalent gate shrinking with $\delta = 0$ only yields a 8% reduction. This is a consequence of the modulating effect of the gate over the Schottky barrier thickness already highlighted in Fig. 3b. When V_{GS} decreases, more holes are induced in the MoS₂ channel, leading to a reduction in the size of the depletion regions associated with the Schottky barriers; this results in a thinning effect on the barriers themselves. In the presence of gate overlaps, the gate is more effective in inducing charge close the NbS₂/MoS₂ interfaces and therefore in thinning the barriers and modulating the current. Finally, in order

TABLE IV: I_{ON}/I_{OFF} for $L_{ch} = 15$ nm at different gate overlap/underlap.

V_{DS} [V]	δ [nm]	I_{ON}/I_{OFF}
-0.6	-2.5	670
-0.6	0.0	1280
-0.6	2.5	1540
-0.8	-2.5	1299
-0.8	0.0	2300
-0.8	2.5	2630

to comprehensively evaluate the potential of the device, we

analyze several dynamic performance metrics that are relevant to a wide range of technological applications. These metrics include the intrinsic delay time (τ), the power-delay product (PDP) and the cut-off frequency (f_t). The intrinsic delay time and power-delay product are the basic figures of merit in digital applications, while the cut-off frequency characterizes the device with respect to radiofrequency applications.

τ and PDP are calculated in a quasi-static approximation using the equations [31]

$$\tau = \frac{Q_{ON} - Q_{OFF}}{I_{ON}}, \quad (3)$$

$$\text{PDP} = (Q_{ON} - Q_{OFF})|V_{DS}|, \quad (4)$$

where Q_{ON} and Q_{OFF} are the total charge in the channel in the ON and OFF states, respectively. The cut-off frequency f_t is evaluated as [31]

$$f_t = \frac{1}{2\pi} \frac{g_m}{C_G} \Big|_{\max(g_m)} \quad (5)$$

where $C_G = \partial Q_{ch}/\partial V_G$ is the total capacitance seen from the gates and $g_m = \partial I/\partial V_G$ is the transistor transconductance. The results are shown in Fig. 5 as a function of the channel length L_{ch} .

The intrinsic delay time as a function of L_{ch} is shown in Fig. 5a. For $L_{ch} > 5$ nm and $\delta = 0$, the intrinsic delay time decreases approximately linearly with L_G . Larger deviations from this behavior are observed for $L_{ch} = 5$ nm, as the values of τ for $V_{DS} = -0.6$ and -0.8 V approximately converge toward a common value of 3.8 ps. The dependence on δ is quantified for $L_{ch} = 15$ nm. A large increase of τ with respect to the case $\delta = 0$ is observed for $\delta = -2.5$, due to the previously discussed I_{ON} degradation.

The power-delay product shown in Fig. 5b increases with increasing V_{DS} and L_{ch} , according to Equation (4). A significant increase is observed in the presence of gate overlaps, which indirectly causes an increase of Q_{ON} by enhancing the coupling between the channel and the contacts.

At fixed V_{DS} , the cutoff frequency shown in Fig. 5c follows a $1/C_G \propto 1/L_{ch}$ behavior. Increasing V_{DS} entails an increase of g_m and, in turn, an increase of f_t . In the presence of gate underlaps, the dependence of the transconductance on V_{DS} becomes much weaker and f_t tends to settle to a common value of ~ 10 GHz.

IV. CONCLUSION

The possibility to fabricate p -type field-effect transistors based on 2D materials is essential to develop a CMOS process using 2D materials as transistor channels. Following recent experimental demonstrations, we have modeled and numerically simulated a p -type transistor based on lateral heterojunctions of MoS₂ and NbS₂ monolayers. The metallic NbS₂ regions act as source and drain extensions, mediating between the MoS₂ channel and the 3D metal contacts of source and drain. Our results indicate that the performance of the device is strongly dependent on the modulation of the Schottky barriers at the MoS₂/NbS₂ interface as a function of both the gate voltage and the drain-to-source bias. In this respect, the gate length and

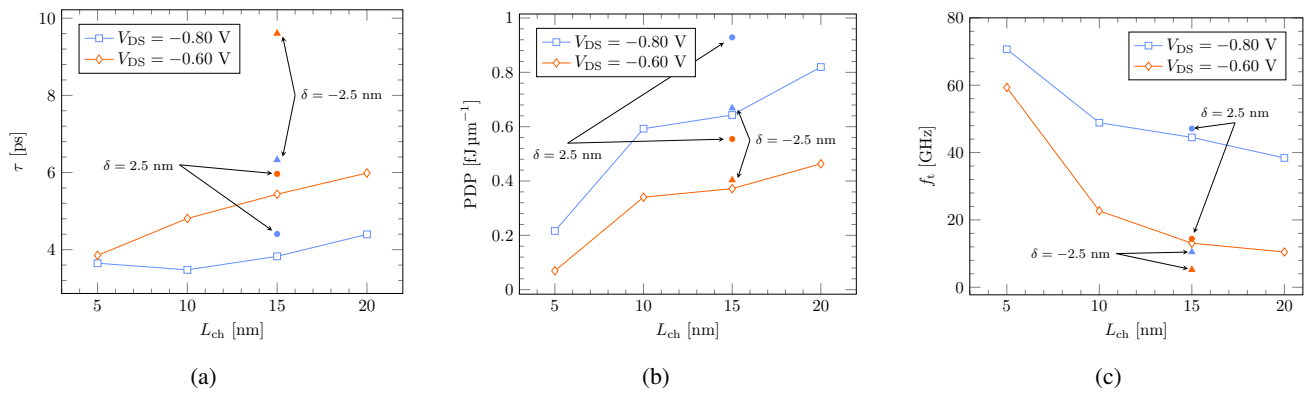


Fig. 5: Dynamic figures of merit of the transistor as a function of the channel length for $V_{DS} = -0.6$ V and -0.8 V. (a) Intrinsic delay time. (b) Power-delay product. (c) Cut-off frequency. In all the cases, the results for a gate overlap (underlap) with $\delta = 2.5$ nm ($\delta = -2.5$ nm) at $L_{ch} = 15$ nm are also shown.

the gate alignment with the $\text{MoS}_2/\text{NbS}_2$ interface prove to be critical parameters to optimize the device performance. These geometrical considerations are expected to have a broader applicability and to describe some general tradeoffs in the design of lateral heterojunction field-effect transistors based on two-dimensional materials.

The scaling behavior shows a strong reduction of the I_{ON}/I_{OFF} ratio at channel lengths of 5 nm, while the dynamic figures of merit remain dominated by capacitive effects and generally improve as the channel shrinks.

The performance of the device under study does not meet the last IRDS projections [19], therefore transistors based on $\text{MoS}_2/\text{NbS}_2$ heterojunctions are not competitive with silicon technology for high-performance logic. An important opportunity can come from 3D integration (i.e., the vertical stacking of planar layers of transistors) because devices based on 2D materials can be fabricated with back-end-of-the-line processes on top of silicon MOSFETs. 3D integration can largely improve the logic function density per unit area, still enabling the use of silicon FETs in circuit locations where the best figures of merit are required. For example, effective non-volatile memories with 2D materials have been demonstrated [32] and do not need to exhibit the typical figures of merit of transistors for high-performance logic circuits. In addition, the interface quality of $\text{MoS}_2/\text{NbS}_2$ heterojunctions can be significantly improved with progress in fabrication techniques [33], yielding better figures of merit.

REFERENCES

- [1] J. Tersoff, "Schottky barrier heights and the continuum of gap states," *Phys. Rev. Lett.*, vol. 52, pp. 465–468, Feb 1984. [Online]. Available: <https://link.aps.org/doi/10.1103/PhysRevLett.52.465>
- [2] L. Yang, K. Majumdar, H. Liu, Y. Du, H. Wu, M. Hatzistergos, P. Y. Hung, R. Tieckelmann, W. Tsai, C. Hobbs, and P. D. Ye, "Chloride molecular doping technique on 2d materials: W_2 and Mo_2 ," *Nano Letters*, vol. 14, no. 11, pp. 6275–6280, 2014, pMID: 25310177. [Online]. Available: <https://doi.org/10.1021/nl502603d>
- [3] A. Allain, J. Kang, K. Banerjee, and A. Kis, "Electrical contacts to two-dimensional semiconductors," *Nature Materials*, vol. 14, no. 12, pp. 1195–1205, Dec 2015. [Online]. Available: <https://doi.org/10.1038/nmat4452>
- [4] D. Jena, K. Banerjee, and G. H. Xing, "Intimate contacts," *Nature Materials*, vol. 13, no. 12, pp. 1076–1078, Dec 2014. [Online]. Available: <https://doi.org/10.1038/nmat4121>
- [5] N. Kaushik, D. Karmakar, A. Nipane, S. Karande, and S. Lodha, "Interfacial n-doping using an ultrathin TiO_2 layer for contact resistance reduction in MoS_2 ," *ACS Applied Materials & Interfaces*, vol. 8, no. 1, pp. 256–263, 2016, pMID: 26649572. [Online]. Available: <https://doi.org/10.1021/acsami.5b08559>
- [6] L. Xie, M. Liao, S. Wang, H. Yu, L. Du, J. Tang, J. Zhao, J. Zhang, P. Chen, X. Lu, G. Wang, G. Xie, R. Yang, D. Shi, and G. Zhang, "Graphene-contacted ultrashort channel monolayer MoS_2 transistors," *Advanced Materials*, vol. 29, no. 37, p. 1702522, 2017. [Online]. Available: <https://onlinelibrary.wiley.com/doi/abs/10.1002/adma.201702522>
- [7] D. S. Schulman, A. J. Arnold, and S. Das, "Contact engineering for 2d materials and devices," *Chem. Soc. Rev.*, vol. 47, pp. 3037–3058, 2018. [Online]. Available: <http://dx.doi.org/10.1039/C7CS00828G>
- [8] X. Cai, Z. Wu, X. Han, Y. Chen, S. Xu, J. Lin, T. Han, P. He, X. Feng, L. An, R. Shi, J. Wang, Z. Ying, Y. Cai, M. Hua, J. Liu, D. Pan, C. Cheng, and N. Wang, "Bridging the gap between atomically thin semiconductors and metal leads," *Nature Communications*, vol. 13, no. 1, p. 1777, Apr 2022. [Online]. Available: <https://doi.org/10.1038/s41467-022-29449-4>
- [9] S. Chen, S. Wang, C. Wang, Z. Wang, and Q. Liu, "Latest advance on seamless metal-semiconductor contact with ultralow schottky barrier in 2d-material-based devices," *Nano Today*, vol. 42, p. 101372, 2022. [Online]. Available: <https://www.sciencedirect.com/science/article/pii/S1748013221002978>
- [10] M. S. Choi, N. Ali, T. D. Ngo, H. Choi, B. Oh, H. Yang, and W. J. Yoo, "Recent progress in 1d contacts for 2d-material-based devices," *Advanced Materials*, vol. 34, no. 39, p. 2202408, 2022. [Online]. Available: <https://onlinelibrary.wiley.com/doi/abs/10.1002/adma.202202408>
- [11] D. S. Schneider, E. Reato, L. Lucchesi, Z. Wang, A. Piacetini, J. Bolten, D. Marian, E. G. Marin, A. Radenovic, Z. Wang, G. Fiori, A. Kis, G. Iannaccone, D. Neumaier, and M. C. Lemme, "MoS₂/graphene lateral heterostructure field effect transistors," in *2021 Device Research Conference (DRC)*, 2021, pp. 1–2.
- [12] C. Kim, I. Moon, D. Lee, M. S. Choi, F. Ahmed, S. Nam, Y. Cho, H.-J. Shin, S. Park, and W. J. Yoo, "Fermi level pinning at electrical metal contacts of monolayer molybdenum dichalcogenides," *ACS Nano*, vol. 11, no. 2, pp. 1588–1596, 2017, pMID: 28088846. [Online]. Available: <https://doi.org/10.1021/acsnano.6b07159>
- [13] Y. Wang, J. C. Kim, R. J. Wu, J. Martinez, X. Song, J. Yang, F. Zhao, A. Mkhoyan, H. Y. Jeong, and M. Chhowalla, "Van der waals contacts between three-dimensional metals and two-dimensional semiconductors," *Nature*, vol. 568, no. 7750, pp. 70–74, Apr 2019. [Online]. Available: <https://doi.org/10.1038/s41586-019-1052-3>
- [14] X. Liu, M. S. Choi, E. Hwang, W. J. Yoo, and J. Sun, "Fermi level pinning dependent 2d semiconductor devices: Challenges and prospects," *Advanced Materials*, vol. 34, no. 15, p. 2108425, 2022. [Online]. Available: <https://onlinelibrary.wiley.com/doi/abs/10.1002/adma.202108425>
- [15] Y. Zhang, L. Yin, J. Chu, T. A. Shifa, J. Xia, F. Wang, Y. Wen, X. Zhan, Z. Wang, and J. He, "Edge-epitaxial growth of 2d NbS_2 - WS_2 lateral metal-semiconductor heterostructures," *Advanced*

- Materials*, vol. 30, no. 40, p. 1803665, 2018. [Online]. Available: <https://onlinelibrary.wiley.com/doi/abs/10.1002/adma.201803665>
- [16] P.-C. Shen, C. Su, Y. Lin, A.-S. Chou, C.-C. Cheng, J.-H. Park, M.-H. Chiu, A.-Y. Lu, H.-L. Tang, M. M. Tavakoli, G. Pitner, X. Ji, Z. Cai, N. Mao, J. Wang, V. Tung, J. Li, J. Bokor, A. Zettl, C.-I. Wu, T. Palacios, L.-J. Li, and J. Kong, "Ultralow contact resistance between semimetal and monolayer semiconductors," *Nature*, vol. 593, no. 7858, pp. 211–217, May 2021. [Online]. Available: <https://doi.org/10.1038/s41586-021-03472-9>
- [17] Q. He, Y. Liu, C. Tan, W. Zhai, G.-h. Nam, and H. Zhang, "Quest for p-Type Two-Dimensional Semiconductors," *ACS Nano*, vol. 13, no. 11, pp. 12 294–12 300, Nov. 2019, publisher: American Chemical Society. [Online]. Available: <https://doi.org/10.1021/acsnano.9b07618>
- [18] Z. Wang, M. Tripathi, Z. Golsanamlou, P. Kumari, G. Lovarelli, F. Mazziotti, D. Logoteta, G. Fiori, L. Sementa, G. M. Marega, H. G. Ji, Y. Zhao, A. Radenovic, G. Iannaccone, A. Fortunelli, and A. Kis, "Substitutional p-type doping in nbs₂-mos₂ lateral heterostructures grown by mcvcd," *Advanced Materials*, vol. 35, no. 14, p. 2209371, 2023. [Online]. Available: <https://onlinelibrary.wiley.com/doi/abs/10.1002/adma.202209371>
- [19] "More moore tables. international roadmap for devices and systems (irds)," <https://irds.ieee.org/editions/2021>, 2021, accessed: 2023-10-04.
- [20] G. Iannaccone, F. Bonaccorso, L. Colombo, and G. Fiori, "Quantum engineering of transistors based on 2d materials heterostructures," *Nature nanotechnology*, vol. 13, no. 3, pp. 183–191, 2018. [Online]. Available: <https://doi.org/10.1038/s41565-018-0082-6>
- [21] J. Kang, H. Sahin, and F. M. Peeters, "Mechanical properties of monolayer sulphides: a comparative study between mos₂, hfs₂ and tis₃," *Physical Chemistry Chemical Physics*, vol. 17, p. 27742, Sep 2015. [Online]. Available: <https://doi.org/10.1039/C5CP04576B5>
- [22] Y. Sun, Z. Zhuo, and X. Wu, "Bipolar magnetism in a two-dimensional nbs₂ semiconductor with high curie temperature," *Journal of Materials Chemistry C*, vol. 6, p. 11401, Oct 2018. [Online]. Available: <https://doi.org/10.1039/C8TC04188A>
- [23] S. Datta, "Nanoscale device modeling: the green's function method," *Superlattices and Microstructures*, vol. 28, no. 4, pp. 253–278, 2000. [Online]. Available: <https://www.sciencedirect.com/science/article/pii/S0749603600909200>
- [24] J. Cao, D. Logoteta, S. Özkaya, B. Biel, A. Cresti, M. G. Pala, and D. Esseni, "Operation and design of van der waals tunnel transistors: A 3-d quantum transport study," *IEEE Transactions on Electron Devices*, vol. 63, no. 11, pp. 4388–4394, 2016.
- [25] D. Logoteta, J. Cao, M. Pala, P. Dollfus, Y. Lee, and G. Iannaccone, "Cold-source paradigm for steep-slope transistors based on van der waals heterojunctions," *Phys. Rev. Res.*, vol. 2, p. 043286, Nov 2020. [Online]. Available: <https://link.aps.org/doi/10.1103/PhysRevResearch.2.043286>
- [26] W. Lee, N. Jean, and S. Sanvito, "Exploring the limits of the self-consistent born approximation for inelastic electronic transport," *Phys. Rev. B*, vol. 79, p. 085120, Feb 2009. [Online]. Available: <https://link.aps.org/doi/10.1103/PhysRevB.79.085120>
- [27] X. Li, J. T. Mullen, Z. Jin, K. M. Borysenko, M. Buongiorno Nardelli, and K. W. Kim, "Intrinsic electrical transport properties of monolayer silicene and mos₂ from first principles," *Phys. Rev. B*, vol. 87, p. 115418, Mar 2013. [Online]. Available: <https://link.aps.org/doi/10.1103/PhysRevB.87.115418>
- [28] M. Lundstrom, *Fundamentals of carrier transport*. Cambridge: Cambridge University Press, 2000.
- [29] J. R. Schaibley, H. Yu, G. Clark, P. Rivera, J. S. Ross, K. L. Seyler, W. Yao, and X. Xu, "Valleytronics in 2d materials," *Nature Reviews Materials*, vol. 1, p. 16055, Aug 2016. [Online]. Available: <https://doi.org/10.1038/natrevmats.2016.55>
- [30] Z. Jin, X. Li, J. T. Mullen, and K. W. Kim, "Intrinsic transport properties of electrons and holes in monolayer transition-metal dichalcogenides," *Phys. Rev. B*, vol. 90, p. 045422, Jul 2014. [Online]. Available: <https://link.aps.org/doi/10.1103/PhysRevB.90.045422>
- [31] F. Mazziotti, D. Logoteta, and G. Iannaccone, "(la, ba)sno₃-based thin-film transistors: Large-signal model and scaling projections," *Phys. Rev. Appl.*, vol. 17, p. 014011, Jan 2022. [Online]. Available: <https://link.aps.org/doi/10.1103/PhysRevApplied.17.014011>
- [32] G. Migliato Marega, Z. Wang, M. Paliy, G. Giusi, S. Strangio, F. Castiglione, C. Callegari, M. Tripathi, A. Radenovic, G. Iannaccone, and A. Kis, "Low-power artificial neural network perceptron based on monolayer mos₂," *ACS Nano*, vol. 16, no. 3, pp. 3684–3694, 2022, pMID: 35167265. [Online]. Available: <https://doi.org/10.1021/acsnano.1c07065>
- [33] J. Wang, Z. Li, H. Chen, G. Deng, and X. Niu, "Recent advances in 2d lateral heterostructures," *Nano-Micro Letters*, vol. 11, p. 48, Jun 2019. [Online]. Available: <https://doi.org/10.1007/s40820-019-0276-y>